Pseudogap of the high-temperature superconductor $La_{1.96-x}Sr_xHo_{0.04}CuO_4$ as observed by neutron crystal-field spectroscopy

Petra S. Häfliger,* Andrew Podlesnyak, Kazimierz Conder, Ekaterina Pomjakushina, and Albert Furrer
Laboratory for Neutron Scattering, ETH Zurich & PSI Villigen, CH-5232 Villigen PSI, Switzerland
(Received 9 March 2006; revised manuscript received 6 July 2006; published 15 November 2006)

We studied the isotope, pressure, and doping effects on the pseudogap temperature T^* by neutron spectroscopic experiments of the relaxation rate of crystal-field excitations in $La_{1.96-x}Sr_xHo_{0.04}CuO_4$ ($x=0.11, 0.15, 0.20, 0.25$). We found clear evidence for the opening of a pseudogap at $T^* > T_c$ in the whole doping range. Furthermore, the effect of oxygen isotope substitution was found to produce an upward shift of T^*, whereas the application of pressure on the optimally doped compound ($x=0.15$) results in a downward shift of T^*. The opposite effect of oxygen isotope substitution and pressure application indicates that electron-phonon induced effects contribute to the pseudogap formation. The temperature dependence of the relaxation data is consistent with a gap function of predominantly *d*-wave symmetry.

DOI: 10.1103/PhysRevB.74.184520 PACS number(s): 74.62.Fj, 74.72.Dn, 76.30.Kg, 78.70.Nx

I. INTRODUCTION

Superconductivity is the result of two distinct quantum phenomena, namely pairing of the charge carriers at a characteristic temperature T^* and long-range phase coherence at the superconducting transition temperature T_c. In conventional superconductors, these two phenomena occur simultaneously, i.e., $T^*=T_c$. In contrast, for high-temperature superconductors we have $T^* > T_c$ over a large doping range, thus the so-called pseudogap region ($T_c < T < T^*$) is clearly the most challenging part of the phase diagram. The experimental discovery of the pseudogap region[1] gave rise to an impressive number of models for the mechanism of high-temperature superconductivity.[2] Consequently, experiments that produce changes of the pseudogap temperature T^* are of crucial importance to discriminate between the different pairing scenarios developed for the cuprate superconductors. In the past, measurements of the isotope effect were essential to establish the BCS model of classical superconductors. Likewise, experiments searching for isotope effects on the pseudogap temperature T^* may be able to discriminate between the different pairing scenarios developed for the cuprate superconductors. X-ray-absorption near-edge spectroscopy (XANES) experiments[3] revealed a huge oxygen isotope effect associated with the onset of local lattice fluctuations in underdoped $La_{1.94}Sr_{0.06}CuO_4$, whose characteristic temperature T^* increases from 110 to 170 K upon replacing ^{16}O by ^{18}O. A large oxygen isotope effect as well as a large copper isotope effect on the pseudogap was also observed by neutron crystal-field spectroscopy for slightly underdoped $HoBa_2Cu_4O_8$ with $T^* \approx 50$ K (Ref. 4) and $T^* \approx 25$ K,[5] respectively. The same technique applied to underdoped, optimally doped, and overdoped $La_{1.96-x}Sr_xHo_{0.04}CuO_4$ (Ho@LSCO) with $x=0.10$, 0.15, and 0.20 yielded oxygen isotope shifts of $T^* \approx 20$, 10, and 5 K, respectively.[6,7] Surprisingly, nuclear magnetic resonance (NMR) and nuclear quadrupole resonance (NQR) experiments resulted in an absence or a very small oxygen isotope shift T^* in $YBa_2Cu_4O_8$,[8,9] which was attributed to the slow time scale of the order of $\tau \approx 10^{-8}$ s.[3,4,10] The large oxygen (and copper) isotope shifts T^* observed by XANES and neutron spectroscopy experiments (which are fast techniques with a time scale of $\tau \approx 10^{-13}$ s) were semiquantitatively accounted for by models based on dynamical charge ordering,[10] phonon-induced stripe formation,[11] and bipolaron formation associated with Jahn-Teller-like oxygen vibrations.[12]

Oxygen isotope effects have been reported on various other quantities; in particular, the oxygen isotope effect on the superconducting transition temperature T_c was investigated in great detail.[13] It is now well established that the doping dependence of the oxygen isotope exponent α_0 is a generic feature of the cuprates.[14–16] In $La_{2-x}Sr_xCuO_4$, α_0 was found to be close to the BCS value of 0.5.[14] Also the in-plane penetration depth is affected by the oxygen isotope substitution, as has been demonstrated by magnetization measurements[14,15] and by muon-spin rotation experiments.[17,18] Furthermore, a large isotope effect on the electron paramagnetic resonance (EPR) linewidth was observed in manganese-doped cuprates.[19] Angle-resolved photoemission spectroscopy (ARPES) data revealed an oxygen isotope effect on the dispersion,[20] which can be explained in a dynamic spin-Peierls picture,[21] where the singlet pairing of electrons and the electron-lattice coupling mutually enhance each other. Additionally, isotope effects on NMR/NQR parameters were observed in $YBa_2Cu_4O_8$.[22,23]

Similarly to isotope substitution, the application of pressure affects the lattice degrees of freedom, thus it could be used as an independent tool to confirm the experimental and theoretical findings concerning T^* described above. Unfortunately, there are only a few pressure-dependent experiments on the pseudogap temperature T^* in the literature, and the results are contradicting. NQR experiments for $YBa_2Cu_4O_8$ (Ref. 24) as well as resisitivity measurements for quenched and Ca-doped $YBa_2Cu_3O_7$ compounds[25] show a (continuous) decrease of T^* with increasing pressure, whereas from the analysis of resisitivity measurements for optimally doped $Hg_{0.82}Re_{0.12}Ba_2Ca_2Cu_3O_{8+\delta}$, a linear increase of T^* with pressure is reported.[26] Recently, neutron spectroscopy experiments under hydrostatic pressure were performed for the optimally doped compound $Ho@La_{2-x}Sr_xCuO_4$.[27] It was found that the pseudogap temperature decreases from $T^* \approx 61$ K at ambient pressure to $T^* \approx 54$ K for $p=1.2$ GPa, i.e.,

$\Delta T^* \approx -7$ K. The opposite effect of pressure application ($\Delta T^* < 0$) and oxygen isotope substitution ($\Delta T^* > 0$) (Refs. 6 and 7) is in qualitative agreement with pairing scenarios that include electron-phonon induced effects.[10–12]

In this work, we summarize the results of neutron spectroscopic investigations of the relaxation rate of crystal-field excitations in $La_{1.96-x}Sr_xHo_{0.04}CuO_4$ in a broad doping range ($0.11 \leqslant x \leqslant 0.25$). Some selected results have already been published.[6,7,27–29] In most high-T_c compounds, interaction at the rare-earth (R) ions are situated close to the superconducting copper-oxide planes, thus the crystal-field interaction at the rare-earth sites constitutes an ideal probe of the local symmetry as well as the local charge distribution of the superconducting CuO_2 planes and thereby monitors directly changes of the carrier concentration induced by ion substitution and external fields. In particular, the intrinsic linewidths of crystal-field transitions are found to vary with temperature, which is essentially a reflection of the density-of-states associated with the charge carriers at the Fermi energy. Linewidth studies can therefore reveal information about the opening as well as the symmetry of the energy gap.

The paper is organized as follows. In Sec. II, the basic principles of neutron crystal-field spectroscopy are summarized. An expression for the observed linewidth is given, and different models for the superconducting gap function and their influences on the linewidth are discussed. In Sec. III, we describe the experimental procedure adopted for the present work. The obtained results are presented in Sec. IV, and their implications for the mechanism leading to high-temperature superconductivity are discussed in Sec. V. Some final conclusions are given in Sec. VI.

II. NEUTRON CRYSTAL-FIELD SPECTROSCOPY AND THE INFLUENCE OF THE NATURE OF THE PSEUDOGAP ON THE RELAXATION RATE

The energy levels of a $4f$ ion in a crystalline lattice are perturbed by the electrostatic potential V_{CF} arising from the neighboring charges at sites $\mathbf{r}_i$,

$$V_{CF} = \sum_i \frac{Z_i e^2}{|\mathbf{r}_i - \mathbf{R}|}, \tag{1}$$

where $\mathbf{R}$ is the rare-earth site. This so-called crystal-field interaction gives rise to discrete energy levels E_k, which can be determined directly by inelastic neutron scattering. For a system of N noninteracting ions, the cross section for the crystal-field transition $\Gamma_l \rightarrow \Gamma_k$ is given in the dipole approximation by[30]

$$\frac{d^2\sigma}{d\Omega d(\hbar\omega)} \sim N\frac{k_f}{k_i}\exp(-2W)F^2(Q)\exp\left(-\frac{E_k}{k_B T}\right)|M_{lk}|^2 \times \delta(E_k - E_l \pm \hbar\omega),$$

$$M_{lk} = \langle \Gamma_k | \hat{J}_p | \Gamma_l \rangle, \tag{2}$$

where k_i and k_f are the wave numbers of the incoming and scattered neutrons, respectively, $\exp(-2W)$ is the Debye-Waller factor, $F(Q)$ is the magnetic form factor, and M_{lk} is the transition matrix element, with $\hat{J}_p$ being the component of the total angular momentum operator perpendicular to the scattering vector $\mathbf{Q}$. The δ function in Eq. (2) is broadened due to the instrumental resolution on the one hand. On the other hand, the crystal-field levels are subject to interactions with phonons, spin fluctuations, and charge carriers, which limit their lifetime, thus the observed crystal-field transitions exhibit line broadening. The δ function in Eq. (2) must therefore be replaced by a convolution of a Gaussian with a Lorentzian. These relaxation aspects will be discussed in the following subsection.

A. Relaxation rate of crystal-field transitions

In rare-earth based high-T_c superconductors, the excited crystal-field levels interact with phonons, spin fluctuations, and charge carriers, which limit the lifetime of the excitations, thus the observed crystal-field transitions exhibit line broadening. Lovesey and Staub[31] put forward the idea that the relaxation rate is dominated by phonon interactions. In their calculation, they neglect all but three of the crystal-field states, which for the case of $Ho_{0.1}Y_{0.9}Ba_2Cu_3O_7$ leads to an unreasonably good agreement with the experimental data.[32] However, the inclusion of the complete set of crystal-field levels produces a drastically different temperature dependence of the linewidth,[32] i.e., the phonon damping picture is no longer supported. Moreover, phonon relaxation exhibits a continuous temperature behavior of the linewidth and cannot reproduce the steplike features observed in several high-T_c cuprates at or above T_c.[33,34] Therefore, we assume that the interaction with the charge carriers is by far the dominating relaxation mechanism.[5] In the normal metallic state, the intrinsic linewidth of a transition between the states $|i\rangle$ and $|j\rangle$ with energy $\hbar\omega_{ij} = \hbar\omega_i - \hbar\omega_j$ is given by[33]

$$\Gamma_n^{ij}(T) = 2J_{ex}^2\left[M_{ij}^2 \coth\left(\frac{\hbar\omega_{ij}}{2k_B T}\right)\chi''(\hbar\omega_{ij}) + \sum_{n\neq i} M_{in}^2 \frac{\chi''(\hbar\omega_{in})}{\exp(\hbar\omega_{in}/k_B T) - 1} + \sum_{n\neq j} M_{nj}^2 \frac{\chi''(\hbar\omega_{nj})}{\exp(\hbar\omega_{nj}/k_B T) - 1}\right], \tag{3}$$

where J_{ex} is the exchange integral between the charge carriers and the $4f$ electrons of the R^{3+} ions, M_{ij} is the transition matrix element of the crystal-field transition $|i\rangle \rightarrow |j\rangle$, and χ'' is the imaginary part of the susceptibility summed over the Brillouin zone. The crystal-field level scheme of Ho^{3+} in $La_{1.96-x}Sr_xCuO_4$ has not been established experimentally so far. But extrapolation from the crystal-field Hamiltonian of $HoBa_2Cu_4O_8$ (Ref. 35) based on the procedure described in Refs. 36 and 37 predicts that the first excited level lies at 0.2 meV, well separated from the next excited levels by about 10 meV. Indeed, the measurements on the MARI spectrometer revealed only one inelastic peak,[29] fully in agreement with the model calculations mentioned above. Hence we can restrict Eq. (3) to the ground-state and the first excited level and expand it up to first order under the assumption $\hbar\omega \ll k_B T$.

We want to point out that $\chi''(\omega)$ is the same local susceptibility as used in nuclear relaxation, i.e., the Brillouin zone sum of $|A(\mathbf{q})|^2\chi''(\mathbf{q},\omega)$, where $\chi''(\mathbf{q},\omega)$ is the dynamic susceptibility probed by neutron scattering and $A(\mathbf{q})$ is a geometrical factor that takes into account the local structure around the lanthanide ion. For a noninteracting Fermi liquid $\chi''(\omega)=\pi N(E_F)^2\omega$, where $N(E_F)$ is the density of states at the Fermi energy E_F, and we will use this form to calculate the normal state linewidth Γ_n. The use of a Fermi liquid model in the present problem is justified by ^{89}Y NMR observations,[38] which show that the ^{89}Y relaxation rate is close to the noninteracting limit in the normal state and obeys the Korringa law. Furthermore, although $\chi''(\mathbf{q},\omega)$ is strongly enhanced around $\mathbf{q}=(\pi/a,\pi/b)$ by antiferromagetic spin fluctuations, these are largely filtered out by $A(\mathbf{q})$, the $\mathbf{q}$ dependence of which reflects that the lanthanide site is a center of symmetry of the fluctuations.[39] This leads, together with the Fermi liquid approach, to the following expression:

$$\Gamma_n(T) = 4\pi M^2 j_{\mathrm{ex}}^2 N^2(E_F) k_B T, \tag{4}$$

which predicts the linewidth to increase linearly with temperature according to the well-known Korringa law[40] in the normal state. In the superconducting state, on the other hand, the pairing of the charge carriers creates an energy gap Δ below the superconducting transition temperature T_c (or a pseudogap below a characteristic temperature T^*), thus crystal-field transitions with energy $\hbar\omega<2\Delta$ do not have enough energy to span the gap, and consequently there is no interaction with the charge carriers. For an isotropic gap, the intrinsic linewidth in the superconducting state is then given by

$$\Gamma_s(T) = \Gamma_n(T)\exp\left(-\frac{\Delta}{k_B T}\right). \tag{5}$$

Below T_c, care has to be taken with $\chi(\mathbf{q},\omega)$, which contains coherence factors arising from the effect on the local susceptibility of superconducting pairing correlations.[41] Such coherence effects influence the NMR relaxation most strongly near T_c, thus Eq. (5) is inappropriate around T_c but may have some approximate validity well below T_c. However, in all our experiments including the YBCO-type compounds,[4] the observed linewidths did not exhibit any anomalies around T_c, but showed a continuous behavior, thus the neglect of the coherence factors may be tolerated. This means that $\Gamma_s(T)\approx 0$ for $T\ll T_c$, and line broadening sets in just below T_c (or T^*) where the superconducting gap (or the pseudogap) opens. Therefore, the corresponding gap (or pseudogap) temperature T_c (or T^*) can be directly derived from the temperature where the linewidth starts to deviate from the Korringa behavior.

Neutron crystal-field spectroscopy has several advantages over other experimental techniques: it is (i) truly bulk-sensitive, (ii) fast in order to be able to detect dynamical effects with a time scale of 10^{-13} s (typical of spin and lattice fluctuations), and (iii) direct in order to reveal a distinct crossover temperature (without involving a complicated mathematical machinery to derive T^* from the raw data). This technique has already been successfully applied to other high-T_c compounds.[4,5,42]

B. Nature of the gap function

It is widely believed that the symmetry of the superconducting order parameter has predominantly d-wave character, and this holds also for the pseudogap.[43] Therefore, the isotropic gap in Eq. (5) has to be replaced by a d-wave gap function of the form

$$\Delta_{x^2-y^2}(\mathbf{k}) \equiv \Delta(\mathbf{k}) = \Delta_0[\cos(k_x)-\cos(k_y)]$$

$$\Leftrightarrow \Delta(\phi) = \Delta_0\cos(2\phi)$$

$$\phi := \arctan\left(\frac{\pi-k_y}{\pi-k_x}\right) \quad 0\leqslant\phi\leqslant\pi/2$$

$$\Delta_0 := \max\Delta(\mathbf{k}), \quad \mathbf{k}\in \text{Fermi surface}. \tag{6}$$

Thus the calculation of $\Gamma_s(T)$ requires an integration in the (k_x,k_y) plane,

$$\Gamma_s(T) = \Gamma_n(T)\oint_{\mathbf{k}_F} dk\, G_k,$$

$$G_k = \begin{cases} 1 & \text{if } \hbar\omega > 2|\Delta(\mathbf{k})| \\ \exp\left(-\dfrac{\Delta(\mathbf{k})}{k_B T}\right) & \text{if } \hbar\omega < 2|\Delta(\mathbf{k})|, \end{cases} \tag{7}$$

where $\mathbf{k}_F$ is the Fermi vector. This procedure has been developed by Mesot *et al.*[44]

However, slight modifications of this general behavior have been observed. Their influences on the relaxation data are presented below and depicted in Fig. 1.

1. Magnitude of the superconducting gap Δ_0

Ido *et al.*[45] found that Δ_0 is closely related to T^* in both BSCCO ($Bi_2Sr_2CaCu_2O_{8+\delta}$) and LSCO ($La_{2-x}Sr_xCuO_4$) systems, namely $T^*\sim 2\Delta_0/4.3k_B$ over a large doping range. However, the size of Δ_0 has only a small influence on the relaxation rate as visualized in panel (a) of Fig. 2.

2. s-wave contribution α to the superconducting gap

A d-wave gap offers relaxation channels even at the lowest temperatures due to the nodes at the azimuthal angle $\phi=45°$ in the gap function. But an s-wave contribution α to the gap shifts these nodes, which can readily be seen from the expression

$$\Delta_0(\mathbf{k},T) = \Delta_0\{(1-\alpha)[\cos(k_x)-\cos(k_y)]+\alpha\}, \tag{8}$$

where $\alpha=1$ stands, therefore, for an isotropic gap as in Eq. (5). Hence in comparison with the linewidth data calculated for a pure d-wave gap, a pure s-wave gap reduces the linewidth substantially at low temperatures, see panel (b) of Fig. 2.

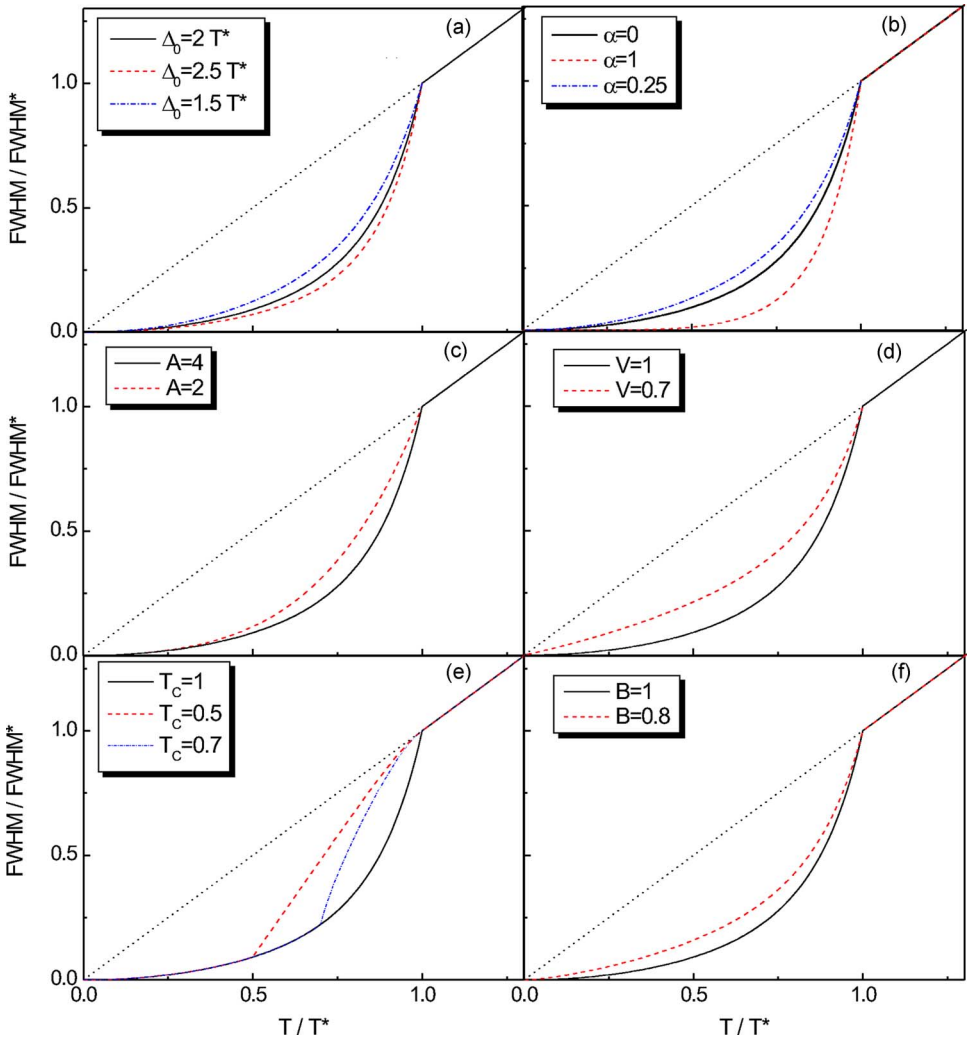

FIG. 1. (Color online) Illustration of the influence of various features of the gap function on the relaxation rate as discussed in the text. (a) Magnitude of the maximum amplitude Δ_0, (b) *s*-wave contribution α to the superconducting gap, (c) temperature exponent A of the gap function, (d) superconducting volume fraction V, (e) gapless Fermi arcs, and (f) contribution of higher harmonics B to the *d*-wave gap.

As long as the amplitude of the *d*-wave gap is larger than the *s*-wave gap, there is still a node in the gap function. However, this node is shifted to a larger angle ϕ and moreover the shape of the gap is no longer symmetric around $\phi = 45°$. Such a behavior has recently been observed in untwinned YBCO[46] by angle-resolved electron tunneling.

In order to quantify the effect of an *s*-wave contribution on the relaxation rate, we recall that the relaxation rate is sensitive to the gap integrated in the reciprocal space. It is therefore helpful to consider the integral gap quantity

$$D(\alpha) = \int_0^{\pi/2} |(1-\alpha)\cos(2\phi) + \alpha| d\phi. \tag{9}$$

Let us define $\alpha_{\min} \in [0,1]$ as the value where $D(\alpha)$ has a minimum. Consequently, the relaxation rate $\Gamma(\alpha_{\min})$ will then be largest. A numerical calculation yields $\alpha_{\min}=0.4$ as displayed in Fig. 2. This means that up to an s-wave contribution $\alpha=0.6$, the linewidth lies, therefore, above the one obtained for a pure *d*-wave as well as for a pure *s*-wave gap.

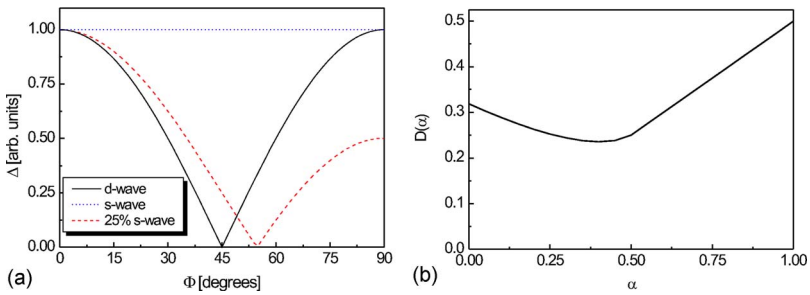

FIG. 2. (Color online) Mixture of *d*- and *s*-wave gap: (a) displays the shape of the gap when 25% *s*-wave character (dashed line) is introduced as compared to a pure *d*-wave gap (solid line) and a pure *s*-wave gap (dotted line). (b) illustrates the behavior of the integral gap quantity $D(\alpha)$, which acquires a minimum for $\alpha_{\min}=0.4$.

An example of how the *s*-wave contribution affects the linewidth is given in Fig. 2(b), where the total gap has been kept constant. It is obvious that an *s*-wave contribution of 25% (α=0.75) has only a small effect.

3. Temperature exponent A of the gap function

The temperature dependence of the gap function can be described by

$$\Delta(\mathbf{k},T) = \Delta(\mathbf{k})\left[1 - \left(\frac{T}{T^*}\right)^A\right]. \tag{10}$$

From ARPES measurements on optimally doped and underdoped BSCCO,[43] we deduce A=4 and 2, respectively. As shown in Fig. 1(c), the size of A has an appreciable effect on the relaxation rate at higher temperatures.

4. Superconducting volume fraction V

Underdoped high-T_c compounds are inhomogeneous, i.e., there are superconducting and nonsuperconducting regions with a superconducting volume fraction,

$$V = \frac{v_s}{v_{\text{tot}}} < 1, \tag{11}$$

where v_s denotes the volume of the superconducting regions and v_{tot} stands for the total volume. $\Gamma(T)$ is then the resulting linewidth as a function of temperature,

$$\Rightarrow \Gamma(T) = \Gamma_s(T)V + \Gamma_n(T)(1-V). \tag{12}$$

Such a phase separation, which was clearly observed, e.g., by neutron crystal-field spectroscopy in $ErBa_2Cu_3O_x$ ($6<x<7$) by Mesot *et al.*,[37,42] has important consequences for the relaxation rate: the relaxation rate is enhanced predominantly at low temperatures due to the Korringa behavior of the nonsuperconducting regions as visualized in Fig. 1(d).

5. Gapless Fermi arcs

Norman *et al.* detected the existence of gapless Fermi arcs in underdoped BSCCO.[47] Their ARPES experiments revealed that on cooling the sample, the pseudogap opens up at different temperatures for different points in momentum space. More specifically, the point nodes of the *d*-wave gap function break up into disconnected arcs that grow in size gradually from T_c to T^*. Since this effect was only observed at a few selected temperatures, we assumed in our model calculation a linear evolution of the size of the gapless arcs with temperature. Gapless Fermi arcs open additional relaxation channels in the pseudogap region, hence the interaction is suddenly increased for $T>T_c$. This results in a kink of the linewidth at T_c.

6. Higher harmonics of the gap function

ARPES experiments performed by Mesot *et al.*[48] revealed the existence of higher *d*-wave harmonics of the gap function in the underdoped region of BSCCO. The gap function then has the form

$$\Delta(\mathbf{k}) \equiv \Delta(\phi) = \Delta_0[B\cos(2\phi) + (1-B)\cos(6\phi)],$$
$$0 \leqslant B \leqslant 1. \tag{13}$$

For underdoped BSCCO (T_C=68 K), Mesot *et al.* found B=0.84, which is significantly below the value B=1 for the optimally doped and overdoped BSCCO.[48] Schnyder *et al.* confirmed these experimental results in their theoretical work using a fermiology approach.[49]

The $\cos(6\phi)$ term in the Fermi surface harmonics can be shown to be closely related to the tight-binding function $\cos(2k_x)-\cos(2k_y)$, which represents next-nearest-neighbor interaction. In the same way, $\cos(2\phi)$ is closely related to the nearest-neighbor interaction. The parameter $B<1$ enhances the relaxation rate in the whole temperature range as visualized in Fig. 1(f).

7. Comparison of various models

As illustrated in Fig. 2, the variation of different parameters of the gap function influences the linewidth in a different manner.

The above presented models can be classified in three categories: (i) models based on different features of the gap function at zero temperature: models (a), (b), and (f) in Fig. 2; (ii) models concerning the temperature behavior of the gap: models (c) and (e) in Fig. 2; and (iii) model referring to special features in real space, such as phase separation, see Fig. 2(d).

It is worth mentioning that both models (d) and (f) lead to a significant increase of the linewidth at low temperatures. Note that in model (d) this effect is produced by an inhomogeneity of the sample, i.e., a real space effect, whereas in model (f) the relaxation is enhanced due to a change in the gap function, i.e., a reciprocal space effect.

Furthermore, the model (c) concerning temperature effects of the gap function changes the relaxation rate predominantly at temperatures near the closing of the pseudogap, while the low-temperature behavior remains almost unaffected.

We will discuss in Sec. V B which models are appropriate and consistent with our relaxation data.

III. EXPERIMENTS

For the present experiments, the polycrystalline $La_{1.96-x}Sr_xHo_{0.04}Cu^{16}O_4$ samples were synthesized by conventional solid-state reaction. A part of every ^{16}O compound was then subjected to ^{18}O diffusion in order to exchange 78% of ^{16}O with its isotope ^{18}O. The details of this process have been worked out by Conder *et al.*[50] The superconducting transition temperatures T_c were determined by ac-magnetic susceptibility measurements and are given in Table I. In $La_{1.96-x}Sr_xHo_{0.04}CuO_4$, the values of T_c are systematically lower than for pure LSCO because of the magnetic pair breaking effect of the holmium ions.

The elastic neutron-scattering experiments were performed on the powder diffractometer HRPT[51] installed at the spallation neutron source SINQ at PSI Villigen.[52] Temperature-dependent diffraction patterns of

TABLE I. Superconducting transition temperature T_c and pseudogap temperature T^* determined for $La_{1.96-x}Sr_xHo_{0.04}CuO_4$. Also the energy of the lowest crystal-field transition $\hbar\omega$ and its residual Gaussian linewidth Γ_g at 1.5 K is given.

x	$T_c(^{16}O)$ (K)	$T_c(^{18}O)$ (K)	$T^*(^{16}O)$ (K)	$T^*(^{18}O)$ (K)	$\hbar\omega_{CEF}$ (meV)	Γ_g (meV)
0.11	13.9±0.3	11.7±0.6	82.2±1.2	103.5±4	0.18±0.005	0.158±0.004
0.15	32.5±0.5	30.8±0.8	61.0±0.5	70.0±1.2	0.185±0.003	0.16±0.004
0.20	28.4±0.6	27.3±0.6	49.2±0.7	53.7±0.6	0.20±0.002	0.164±0.005
0.25	10.1±0.2	9.8±0.2	46.5±0.5	48.4±1.4	0.208±0.002	0.174±0.004
0.15 (p=1 GPa)	33.2±0.3					
0.15 (p=0.8 GPa)			55.8±1.3		0.191±0.005	
0.15 (p=1.2 GPa)			54.1±1.3		0.191±0.005	

$La_{1.81}Sr_{0.15}Ho_{0.04}Cu^{18}O_4$ were obtained at an incident neutron wavelength of 1.9 Å. The diffraction patterns taken at 15 and 100 K are shown in Fig. 3.

The inelastic neutron-scattering experiments were performed on the high-resolution time-of-flight spectrometer FOCUS[53] at SINQ, PSI Villigen. FOCUS was operated at an incident wavelength of 5.75 Å, which means under identical conditions as described in Ref. 6. The samples were enclosed in Al cylinders mounted in a He cryostat to achieve temperatures $T \geqslant 1.5$ K. In order to apply hydrostatic pressure, we used an axially symmetric pressure cell made of hardened aluminum,[54] where we inserted the sample and the pressure medium Fluorinert FC-77. We performed a diffraction experiment with sodium chloride for the calibration of applied pressure. Measurements were also carried out for the empty sample container and the empty pressure cell in order to correct the data for background effects by subtraction.

The left panel of Fig. 4 shows a typical energy spectrum of neutrons scattered from $La_{1.76}Sr_{0.20}Ho_{0.04}Cu^{18}O_4$ at T =10 K. It is similar to the spectra measured for the other investigated compounds. There are strong ground-state crystal-field transitions for both the Stokes and the anti-Stokes process at an energy transfer $\hbar\omega \approx \pm 0.2$ meV. The width of the crystal-field transitions being typically 160 μeV is considerably broader than the instrumental resolution of 50 μeV at the given wavelength: the enhanced width arises from local structural distortions around the Ho^{3+} ions resulting from the doping with Sr^{2+} ions. The lines in Fig. 4 (left panel) are the result of a least-squares-fitting procedure in which the crystal-field transitions were described by a convolution of a temperature-independent Gaussian function (corresponding to the residual low-temperature width) with a temperature-dependent Lorentzian function describing the intrinsic linewidth due to the interaction with the charge carriers. With increasing temperature, the crystal-field transitions renormalize due to relaxation effects: the energy $\hbar\omega$ decreases as shown in Fig. 5 and simultaneously the linewidths increase. This opposite behavior of the energy $\hbar\omega$ and the linewidth is nicely displayed in the right panel of Fig. 4.

We observed that the crystal-field transition exhibits a doping dependence: $\hbar\omega$ slightly increases with raising doping, see Table I. Also the application of pressure leads to an enhancement of $\hbar\omega$ up to ±0.191 meV. Table I also gives the residual low-temperature linewidth; we found an increase with doping.

IV. RESULTS

A. Structural properties

The diffraction patterns taken for $La_{1.81}Sr_{0.15}Ho_{0.04}Cu^{18}O_4$ at 15 and 100 K were refined by using the Rietveld method, yielding a good agreement between the observed and the calculated intensities, see Fig. 3. Clearly both data sets correspond to the low-temperature orthorhombic (LTO) phase (space group *Cmca*). The refined parameters are in good agreement with the results for pure $La_{1.81}Sr_{0.15}CuO_4$ reported by Radaelli *et al.*,[55] which means that a content of 4% holmium did not induce a phase transition from LTO to a tetragonal LTT structure. We also checked the structure at room temperature, where we confirmed the high-temperature tetragonal (HTT) phase in agreement with literature data.[55]

B. Results for the pseudogap temperature T^*

Figure 6 shows the temperature dependence of the intrinsic linewidths Γ=FWHM (full width at half-maximum) for $La_{1.96-x}Sr_xHo_{0.04}Cu^{16}O_4$ at different doping levels (x=0.11, 0.2, and 0.25). They all show a qualitatively similar behavior: the linewidth is rather small at low temperatures, then it raises with increasing slope $d\Gamma/dT$ up to about 70–80 and 45–50 K for the underdoped and overdoped doping levels,

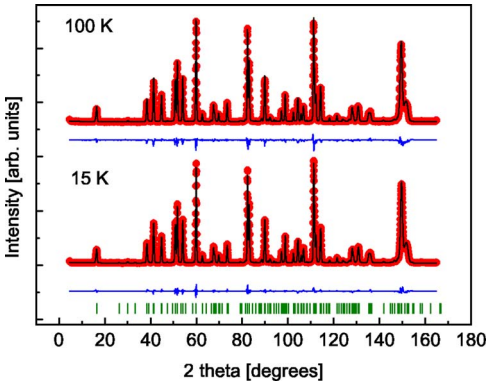

FIG. 3. (Color online) Neutron-diffraction patterns for $La_{1.81}Sr_{0.15}Ho_{0.04}Cu^{18}O_4$ at T=15 and 100 K. The experimental data are shown by red circles, the solid line is the result of the Rietveld refinement. The difference between the calculated and observed patterns is given by the blue line. The bars denote the Bragg reflections.

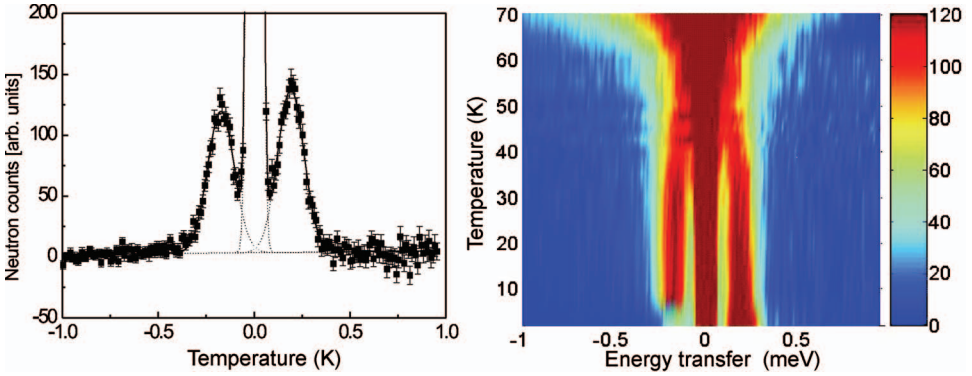

FIG. 4. (Color) Left panel: Energy spectrum of neutrons scattered from $La_{1.76}Sr_{0.20}Ho_{0.04}Cu^{18}O_4$ at $T=10$ K. The solid line is a fit to the data, which include the relaxation as described in the text. The dotted lines illustrate the subdivision into the crystal-field transitions and the elastic line. Right panel: Intensity contours visualizing the temperature renormalization of the energy spectra taken for $La_{1.76}Sr_{0.20}Ho_{0.04}Cu^{18}O_4$.

respectively; from thereon the slope $d\Gamma/dT$ is reduced and remains constant according to the Korringa law. From these observations we can immediately conclude that the pseudogap opens at approximately 80 and 45–50 K in the underdoped and overdoped region, respectively. The comparison to the raw linewidth data taken for the ^{18}O compound also suggests a positive oxygen isotope effect on the pseudogap temperature T^*, since the turnover into the Korringa regime seems to occur for the ^{18}O data at a higher temperature than for the ^{16}O data. Both T^* and ΔT^* decrease with increasing doping.

Similar data were obtained for $La_{1.81}Sr_{0.15}Ho_{0.04}CuO_4$ under pressure, see Fig. 7. The application of hydrostatic pressure slightly lowers T^*, as can be seen in Fig. 7. However, due to the limited number of linewidth data, the quantitative assessment of the pseudogap temperature T^* needs some more detailed considerations of the linewidth in the superconducting state as well as in the pseudogap state. We follow the procedure described in Ref. 28 and outlined below.

In our fitting procedure we describe the linewidth below T^* by a d-wave gap function according to Eqs. (6) and (8). Above T^*, the linewidth is governed by Eq. (4). The independently adjustable parameters of the least-squares-fitting procedure are then T^*, Δ_0, and the slope $d\Gamma/dT$ of the Korringa line. The results of the fitting procedures are shown by solid lines in Figs. 6 and 7. We find a decrease of T^* from 82.2 ± 1.2 to 49.2 ± 0.7 K down to 46.5 ± 0.5 K for $x=0.11$, 0.2, and 0.25, respectively. The optimally doped sample ($x=0.15$) has already been investigated earlier[6] and T^* turned out to be 61.0 ± 0.5 K, which coincides with the charge ordering temperature.[56] The oxygen isotope substituted samples show the same behavior except that T^* is systematically higher. The isotope effect ΔT^* is most pronounced at the lowest doping level where the ratio $\Delta T^*/T^*(^{16}O)$ equals 26%; it decreases to 14% and 10% at $x=0.15$ and 0.2, respectively, and finally vanishes in the heavily overdoped regime. The results are summarized in Table I, see also Refs. 7 and 28.

Figure 7 illustrates the relaxation data taken for $La_{1.81}Sr_{0.15}Ho_{0.04}CuO_4$ at ambient pressure and at 0.8 and 1.2 GPa. The pressure-induced shift of the pseudogap temperature in optimally doped LSCO turned out to be $\Delta T^*=(-5.2\pm2.8)$ and (-6.9 ± 2.8) K at $p=0.8$ and 1.2 GPa, respectively. From these results we derive the pressure effect on T^* to be $\partial T^*/\partial p=(-5.9\pm1.6)$ K/GPa. Our result is in reasonable agreement with $dT^*/dp\approx-10$ K/GPa determined for slightly underdoped $YBa_2Cu_4O_8$ in NQR measurements.[24] We can definitely rule out an increase of T^* with pressure, as has been reported for optimally doped $Hg_{0.82}Re_{0.12}Ba_2Ca_2Cu_3O_{8+\delta}$ from the analysis of resistivity measurements.[26]

V. DISCUSSION

A. Crystal-field excitations in $La_{1.96-x}Sr_xHo_{0.04}CuO_4$

So far the crystal-field interaction of Ho^{3+} in $La_{2-x}Sr_xCuO_4$ has not been established experimentally. Therefore, we derived the crystal-field parameters by extrapolation from those of $HoBa_2Cu_3O_7$ (Ref. 57) based on the procedure described in Ref. 36 and using the structural parameters for $HoBa_2Cu_3O_7$ (Ref. 58) and $La_{2-x}Sr_xCuO_4$.[55] This extrapolation procedure predicts the first-excited crystal-field level to lie at 0.25 meV, separated from the next excited levels by about 10 meV. The transition matrix elements of the latter are at least an order of magnitude smaller

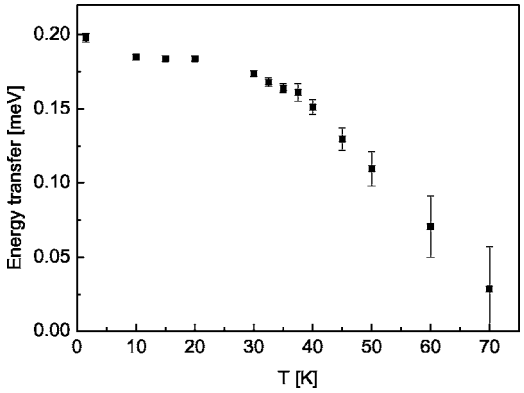

FIG. 5. Renormalization effects of the lowest ground-state crystal-field transition in $La_{1.71}Sr_{0.25}Ho_{0.04}Cu^{18}O_4$.

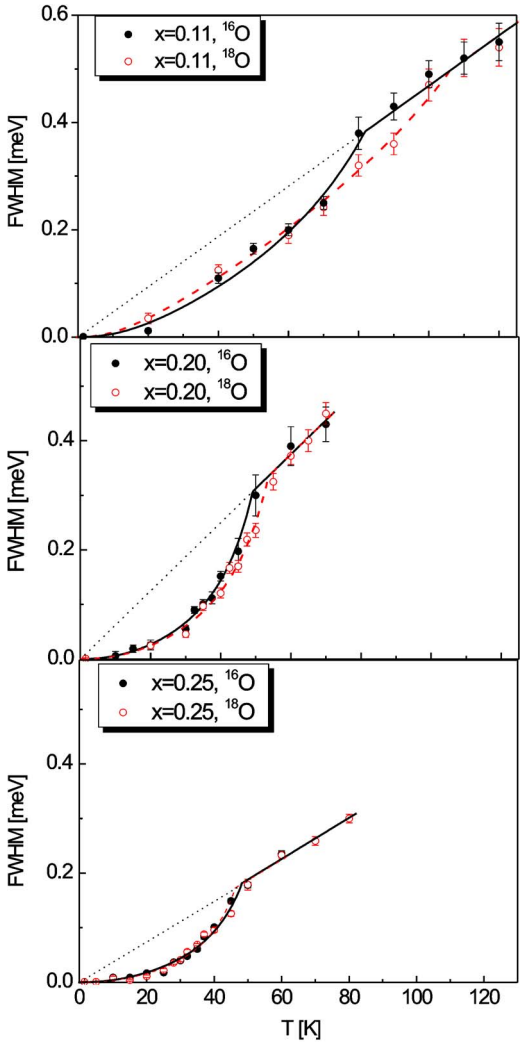

FIG. 6. (Color online) Temperature dependence of the intrinsic linewidth (FWHM) corresponding to the lowest ground-state crystal-field transition in $La_{1.96-x}Sr_xHo_{0.04}CuO_4$ at different doping levels: $x=0.11$ (left panel), $x=0.2$ (middle panel), and $x=0.25$ (right panel). The black full and red open circles correspond to the ^{16}O and ^{18}O compound, respectively. The full and dashed lines are the results of a least-squares-fitting procedure to the ^{16}O and ^{18}O data, respectively, as described in the text. The dotted lines indicate the Korringa behavior below T^*.

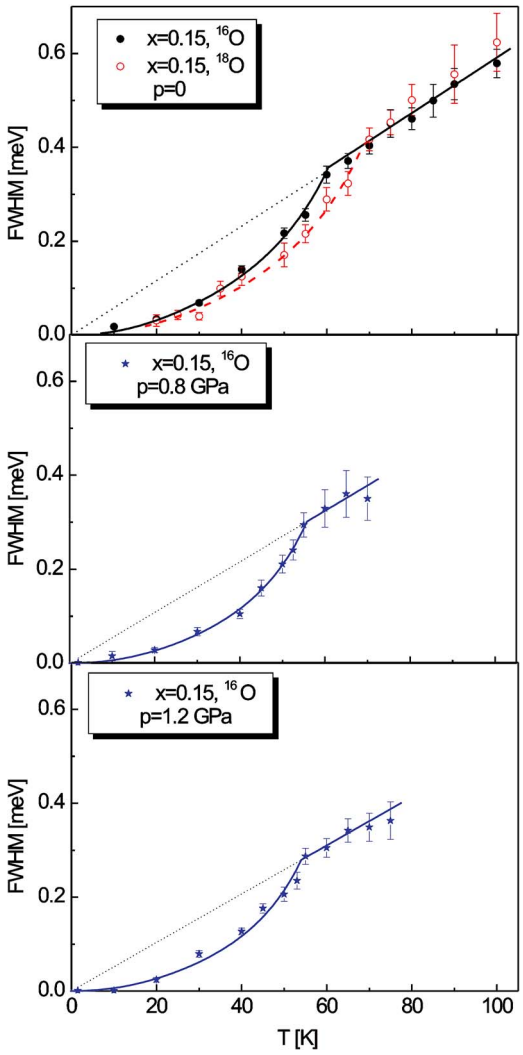

FIG. 7. (Color online) Temperature and pressure dependence of the intrinsic linewidth (FWHM) corresponding to the lowest ground-state crystal-field transition in $La_{1.81}Sr_{0.15}Ho_{0.04}Cu^{16}O_4$. The full lines are the results of a least-squares-fitting procedure as described in the text. The dotted lines indicate the Korringa behavior below T^*.

than for the lowest crystal-field transition observed in the present work, which was recently confirmed by neutron spectroscopic experiments.[29]

Equation (1) shows that the crystal-field potential is a function of both the structure and the charge distribution. In the point-charge approximation, the crystal-field parameters are given by[59]

$$A_n^m = e|e|\langle r^n\rangle \sum_i Z_i \gamma_{nm}(i) \tag{14}$$

with

$$\gamma_n^m(i) = f_n^m\left(\frac{\theta_i, \phi_i}{(\mathbf{r}-\mathbf{R}_i)^{n+1}}\right). \tag{15}$$

The sum i runs over all neighboring ions at position $\mathbf{R}_i = (R_i, \theta_i, \phi_i)$, $f_n^m(\theta_i, \phi_i)$ are tesseral harmonics, $\langle r^n\rangle$ is the nth moment of the radial distribution of the $4f$ electrons, Z_i is the charge of the ith ligand ion in units of the electron charge $|e|$, and $\gamma_n^m(i)$ are the geometrical coordination factors as defined, e.g., by Hutchings.[59] In high-T_c superconductors, the crystal-field potential is mainly determined by the nearest-neighbor oxygen shell (see, e.g., Ref. 36), thus we include in the calculation of the geometrical coordination factors $\gamma_n^m(i)$ the four O(1) ions in the Cu plane and the five O(2) ions in the (La,Sr,Ho) plane.

Figure 8 shows the evolution of the observed ground-state CEF splittings $E_{obs}(x)$ whose sizes raise continuously with increasing Sr doping x. The figure also shows the modification of the CEF splittings $E_{cal}(x)$ calculated from the structural changes on the basis of the procedure described above. We recognize that the structural changes alone cannot repro-

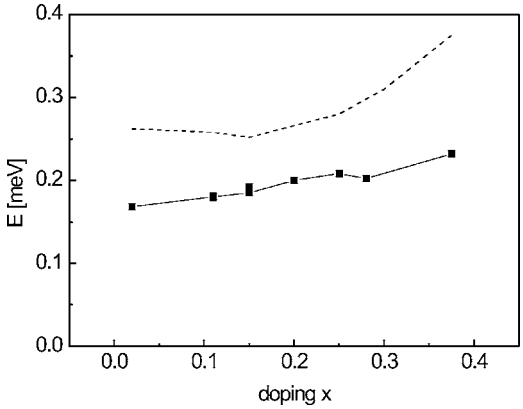

FIG. 8. Ground-state crystal-field splittings observed for $Ho@La_{2-x}Sr_xCuO_4$ (squares and solid curves). The values extrapolated from the structural changes alone are indicated by the dashed curves.

duce the experimental data in a broad doping range ($0.1 < x < 0.3$): In the underdoped region up to $x=0.15$, the experimental values E_{obs} increase, whereas the calculated values E_{calc} decrease. This opposite behavior indicates clearly that the charge transfer is most prominent in this doping region, i.e., additional charges $\delta(x)$ are transferred to the oxygen sites due to Sr doping, according to Eqs. (14) and (15). For doping levels $x \geqslant 0.15$, E_{obs} and E_{calc} both have the same tendency (they are enhanced with increasing doping). The charge transfer $\delta(x)$ can be estimated according to

$$\frac{E_{obs}(x)}{E_{obs}(x=0.02)} = [1+\delta(x)]\frac{E_{cal}(x)}{E_{cal}(x=0.02)}. \tag{16}$$

The resulting charge transfers $\delta(x)$ are listed in Table II. We recognize that the values of $\delta(x)$ follow nicely the x-dependent changes of the slope of the Korringa line $d\Gamma/dT$, which is a measure of the density of states of the charge carriers. Moreover, a similar correspondence follows from a comparison of the values of $\delta(x)$ with the electronic specific-heat coefficients γ (Ref. 60), which are also directly related to the carrier density. Therefore, we conclude that both the observed crystal-field splittings and the observed slopes of the Korringa line are qualitatively consistent with the established picture of charge transfer by doping. For Sr dopings up to $x=0.20$, the charge transfer increases almost linearly, however, this relationship clearly no longer holds in the heavily overdoped region ($x > 0.20$).

TABLE II. Charge transfer $\delta(x)$ and changes of the slope of the Korringa line derived in the present work for $Ho@La_{2-x}Sr_xCuO_4$, in comparison with the electronic specific-heat coefficients γ (Ref. 60). The values of $\delta(x)$ and $\delta(d\Gamma/dT)(x)$ are normalized to zero for $x=0.02$.

x	$\delta(x)$	$\delta(d\Gamma/dT)(x)$	$\gamma(x)$ (mJ/mol K^2)
0.02	0	0	2
0.11	0.09±0.03	0.7±0.7	6
0.15	0.14±0.02	1.9±0.7	9
0.20	0.17±0.01	2.2±0.6	14
0.25	0.16±0.01	−0.2±0.7	12.5
0.28	0.03±0.01	−1.3±1.1	11
0.375	−0.03±0.01	−0.7±1.2	

Upon application of hydrostatic pressure, the crystal-field transition increases from $\hbar\omega=(\pm 0.185\pm 0.003)$ at ambient pressure up to $\hbar\omega=(\pm 0.191\pm 0.005)$ at $p=1.2$ GPa, which can be reproduced using the above-mentioned extrapolation scheme based on structural parameters[55,61] alone. Thus there is no charge transfer induced by pressure, which is in agreement with the Hall coefficient being independent of pressure.[62] However, the slope of the Korringa line $d\Gamma/dT$ decreases slightly with raising pressure from (5.8 ± 0.1) μeV/K at ambient pressure down to (5.2 ± 0.1) μeV/K at 1.2 GPa, which means that j_{ex} is affected by pressure according to Eq. (4).

Let us now discuss the temperature-independent line-broadening mechanisms. The crystal-field interaction is a local probe and thereby sensitive to local structural distortions around the Ho ions. The nearest-neighboring (La,Sr)-coordination shell around a Ho ion comprises a total of eight La and Sr ions, the detailed distribution of La and Sr ions being strongly dependent on the Sr concentration x.

The La and Sr ionic radii are different, which results in a geometrical distortion; in fact, detailed structural investigations performed by Radaelli *et al.*[55] show that the lattice parameter a decreases with increasing Sr content x, whereas the lattice parameter c increases at the same time. Therefore, with the crystal field being a local probe, the positions of the crystal-field transition will be dependent on β at a given doping x.

Assuming the La and Sr ions to be statistically distributed, the following expression gives the probability for a Ho ion having at least one Sr or Ho ion in its coordination shell, which will therefore be distorted:

$$P(x) = \sum_{\beta=1}^{8} p_\beta(x), \tag{17}$$

$$p_\beta(x) = \binom{8}{\beta}\left(\frac{x}{2}\right)^{8-\beta}\left(1-\frac{x}{2}\right)^{\beta}. \tag{18}$$

Thus the probability that a Ho ion has neither a Sr nor another Ho ion in its coordination shell is given by

$$\bar{P}(x) = 1 - P(x) = p_0(x) = \frac{x}{2}^8. \tag{19}$$

In these equations, the binomial coefficients indicate the multiplicity of possible (La,Sr) configurations. Thus the probability that a Ho ion experiences a distorted environment is enhanced while doping increases; see Table III.

The probability of β Sr or Ho ions being in the coordination shell decreases rapidly with β and the decrease is faster the lower the doping; see Fig. 9. Therefore, we expect the line broadening to be most pronounced at higher doping because of the weighted sum of all the different crystal-field

TABLE III. Probability $\bar{P}(x)$ that a Ho ion has a coordination shell that is geometrically distorted due to the presence of at least one Sr or Ho ion.

x	0.11	0.15	0.2	0.25
$\bar{P}(x)$	0.364	0.464	0.570	0.656

contributions. Indeed, the low-temperature residual width is growing with doping and it is 10% larger at $x=0.25$ than at $x=0.11$.

B. The pseudogap in $La_{1.96-x}Sr_xHo_{0.04}CuO_4$

A summary of our results is displayed in Fig. 10. The doping dependence of T^* established from our experiments shows the widely accepted decrease with growing Sr content. In particular, our results up to optimal doping are in good agreement with susceptibility, resistivity, and specific-heat measurements[45] as well as NQR experiments.[56]

For the overdoped region, the situation concerning T^* is controversial. For $x=0.20$, our value of $T^* \approx 50$ K is confirmed by heat capacity[45,63] and resistivity[45] data, whereas NQR data[56] give a slightly reduced $T^* \approx 35$ K. For $x \geqslant 0.22$, however, the analysis of heat capacity data[45] suggests the T^* line merges with the T_c line. Furthermore, by analyzing the resistivity data, Tallon and Loram[64] conclude that the T^* line intersects the T_c line already at $x=1/8$ and vanishes for $x \geqslant 0.18$. This means that our value of $T^* \approx 45$ K for $x=0.25$ could not be confirmed by any other experiments so far.

We discuss now the observed shifts of T^* upon oxygen isotope substitution and pressure application on a semiquantitative level. In a first approximation, the phonon energy $h\nu$ of the active phonon mode is inversely proportional to the square root of the oxygen mass. Thus we find $\Delta h\nu = -0.057$ upon oxygen isotope substitution, whereas the application of pressure leads to $\partial(h\nu)/(h\nu)\partial p = -\gamma\kappa = +0.014$, with $\gamma \approx 2$ being the Grüneisen parameter and $\kappa = -6.8 \times 10^{-3}$ GPa^{-1} the volume compressibility.[61] The opposite effects of isotope substitution and pressure on the phonon energy $h\nu$ implicates

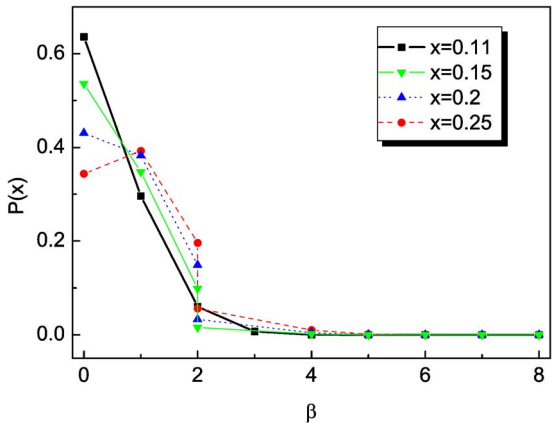

FIG. 9. (Color online) Probability $p_\beta(x)$ for Ho having a distorted shell for different doping levels as a function of β, the number of Sr ions in its coordination shell.

an opposite effect on T^* within models based on phonon-mediated mechanisms:[10–12] The thermodynamic relation

$$\frac{\partial \ln[T^*(p)]}{\partial p} \approx \beta \frac{\partial \ln[\hbar\omega_p(0)]}{\partial p} = -\beta\gamma\kappa \tag{20}$$

with the scaling factor β yields then a pressure effect $\partial T^*/\partial p = (-2.5 \pm 0.9)$ K/GPa as explained in detail in Ref. 28.

These semiquantitative considerations explain the opposite effects of isotope substitution and pressure. However, lattice fluctuations alone cannot explain the measured pressure effect $\partial T^*/\partial p$; they account for only half of the experimentally observed decrease of T^*. Other contributions to $\partial T^*/\partial p$ arise from the pressure dependence of the antiferromagnetic fluctuations, because pressure modifies the structure and therefore affects the superexchange between the copper ions. Unfortunately, there are no experimental data or theoretical predictions available on the pressure dependence of the superexchange coupling J and the hopping integral t being the main ingredients of the t-J model,[65,66] which is based on antiferromagnetic spin fluctuations.

C. Nature of the gap function

To our knowledge, there are no direct experimental results available either on the nature of the gap function or on the temperature evolution of the pseudogap in LSCO. Below, we will outline some characteristics of the superconducting gap function based on our relaxation data, and we will discuss the plausibility of the different models described in Sec. II. These considerations, however, have to be considered with caution for the following reasons: (i) there are too many parameters and effects that influence the temperature dependence of the relaxation rate; (ii) many parameters have a similar effect on the relaxation data; (iii) our model calculations are based on a rather crude approximation for the local

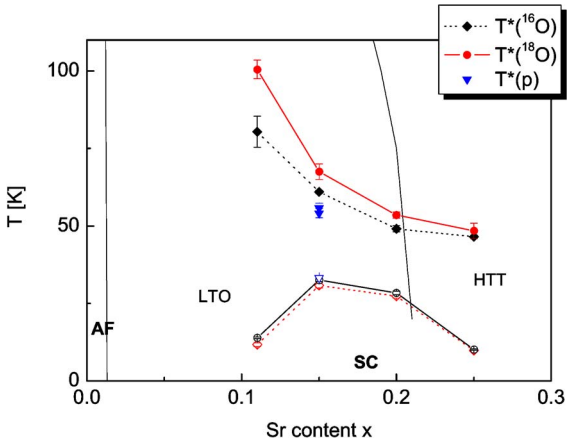

FIG. 10. (Color online) Values for the pseudogap temperature T^* obtained by neutron crystal-field spectroscopy. The black diamonds and red circles stand for T^* of the ^{16}O and ^{18}O compound, respectively. The blue triangles denote the values of T^* obtained under pressure (0.8 and 1.2 GPa). The open circles (diamonds) denote the superconducting transition temperature T_c of the ^{16}O (^{18}O) compound, whereas the blue triangle stands for T_c under pressure.

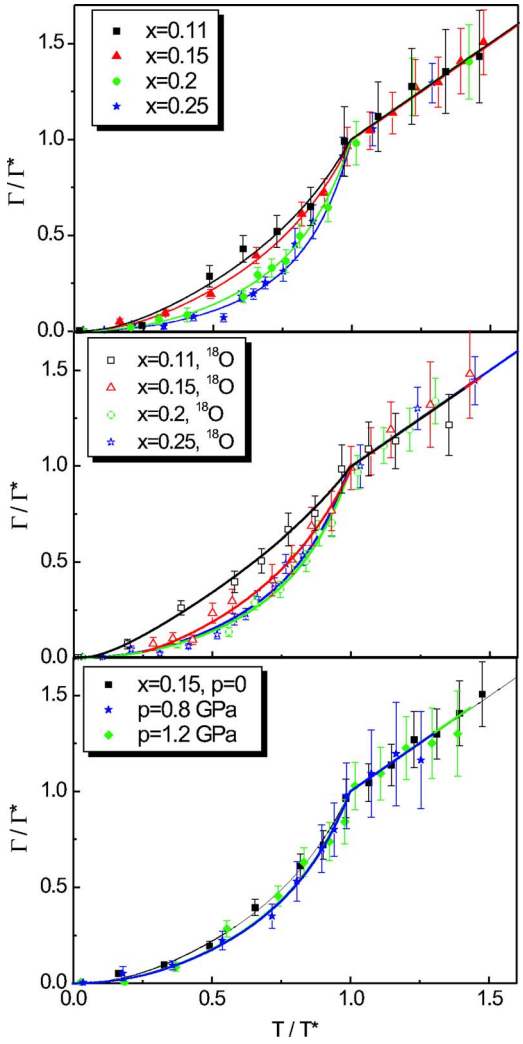

FIG. 11. (Color online) The relaxation data for Ho@LSCO observed in the present work are shown in reduced units Γ/Γ^* vs T/T^* for different doping levels for the ^{16}O compound (upper panel), the ^{18}O compound (middle panel), and for the application of pressure (lower panel).

susceptibility (neglect of the coherence factor around T_c). Therefore, our conclusions may not be completely unambiguous. However, our model calculations were motivated by the need to have a mathematical tool to describe the relaxation data rather than to obtain a detailed insight into the nature of the gap function. This is best exemplified by the model parameter Δ_0, whose value is always slightly below the empirical rule $\Delta_0 \approx 2k_BT$ established for LSCO.[45]

Figure 11 presents a summary of the relaxation data, where the data are plotted in reduced units Γ/Γ^* as a function of T/T^*, where we defined $\Gamma^* \equiv \Gamma(T^*)$. It is eye-catching that the shape of the electronic excitation spectrum in the pseudogap region is dependent on doping: the smaller the doping, the less gapped the relaxation data. The reasons for that experimental result can be manifold.

There are three main characteristics in the doping dependence of the relaxation rates for the ^{16}O compound displayed in the upper panel of Fig. 11.

(i) The doping affects Γ/Γ^* in the whole temperature range $0<T<T^*$. Such a behavior is inconsistent with a variation of the temperature exponent A of the gap function [see Fig. 2(c)], but it can be attributed either to changes in the gap amplitude Δ_0, an s-wave contribution α to the gap function, changes in the superconducting volume fraction V, or the contribution of higher harmonics B to the d-wave gap as illustrated in Figs. 2(a), 2(b), and 2(d) or 2(f), respectively.

(ii) The relaxation rates become finite even at very low temperatures, thus we can rule out a pure s-wave gap for all doping levels; see Fig. 2(b).

(iii) Since there is no clear indication of any anomalies around T_c in the relaxation rate (partly due to the lack of a sufficient number of data points), we no longer consider the picture of gapless Fermi arcs [see Fig. 2(e)], which, however, were used in the interpretation of the relaxation data taken for $HoBa_2Cu_4O_8$.[67]

The relaxation data in reduced units are also presented for the ^{18}O compounds (middle panel of Fig. 11) as well as for the results of the pressure experiments (lower panel of Fig. 11). For the case of the oxygen isotope substituted compounds, we observe a suppression of the relaxation rate with increasing doping, similar to the ^{16}O data within the experimental uncertainty. Both data sets show the characteristics stated above. The application of hydrostatic pressure does not affect the relaxation rate within the range of errors.

In our fitting procedure we consider the gap amplitude Δ_0, the pseudogap temperature T^*, and the slope of the Korringa line $d\Gamma/dT$ as the major fitting parameters where we keep the temperature exponent of $\Delta(\mathbf{k},T)$ fixed at $A=4$; see Eq. (10). The remaining parameters are set at some reasonable values taken from other experiments as explained below.

In principle, the growing of the linewidth as doping decreases can be interpreted by a small s-wave contribution to Δ_0, as has been found in Ref. 46. Since a nonvanishing oxygen isotope effect on T^* is believed to implicate a phonon contribution to the pseudogap formation, where the electron-phonon interaction is isotropic, the superconducting gap must contain an s-wave contribution $1-\alpha$. We therefore set up the following constraint ΔT^*:

$$\frac{\Delta T^*}{T^*} \approx \frac{\alpha}{1-\alpha}. \tag{21}$$

It has been shown repeatedly that underdoped high-T_c compounds are inhomogeneous, i.e., superconducting and antiferromagnetic domains coexist as evidenced by an incomplete Meissner fraction of the superconducting state (see, e.g., Refs. 68 and 69). As a result, the onset of bulk superconductivity results from a percolation mechanism. We therefore introduce an incomplete superconducting volume fraction $V<1$ for the underdoped compounds in our model calculations.

Finally, we include higher harmonics into the gap function up to the optimum doping, i.e., for the underdoped region we use values $B<1$ as observed for underdoped BSCCO.[48,49]

The parameters used for the fitting procedure of the relaxation data are summarized in Table IV. With these param-

TABLE IV. Fitting parameters for $La_{1.96-x}Sr_xHo_{0.04}CuO_4$ using a nonsuperconducting volume fraction V and the inclusion of higher harmonics $1-B$ as explained in the text.

x	Δ_0 (K)	$1-\alpha$	$d\Gamma/dT$ (μeV/K)	B	V
0.11	1.60±0.2	0.25	4.7±0.2	0.85	0.75
0.15	1.40±0.2	0.15	5.9±0.2	0.95	0.9
0.20	1.55±0.1	0.10	6.2±0.1	1	1
0.25	1.5±0.1	0.0	3.8±0.2	1	1

eters, we are able to reproduce the observed relaxation data in a satisfactory manner; see Fig. 11.

VI. CONCLUSIONS

We applied neutron crystal-field spectroscopy systematically to $La_{1.96-x}Sr_xHo_{0.04}CuO_4$ ($0.11 \leqslant x \leqslant 0.25$) in order to study the effects of doping, oxygen isotope substitution, and pressure application at the Ho^{3+} sites, which are situated close to the superconducting copper-oxide planes. More specifically, we were able to determine directly the pseudogap temperature T^* from the temperature dependence of the linewidth of the lowest-lying crystal-field transition associated with the Ho^{3+} ions. We found clear evidence for the existence of the pseudogap in the whole doping range, even for the heavily overdoped compound ($x=0.25$).[28] T^* gradually decreases with increasing doping, and we have $T^* > T_c$ for all doping levels. The oxygen isotope substituted samples exhibit a similar behavior, however the values of T^* are systematically higher. The isotope effect ΔT^* decreases with increasing doping and vanishes eventually for the heavily overdoped sample ($x=0.25$). The application of pressure to the optimally doped sample results in a downward shift of T^*.

We would like to point out that the observed reduction of the linewidth and therefore the suppressed interaction with the charge carriers is a purely dynamic effect, because there is no structural phase transition in the low-temperature regime ($T \leqslant 100$ K). Hence the sudden decrease of the relaxation rate at T^* clearly originates from the opening of the pseudogap.

Our relaxation data suggest that the superconducting gap has generally d-wave symmetry. For the interpretation of the relaxation data in the underdoped regime, we had to include some doping-dependent effects, namely the existence of a nonsuperconducting volume fraction as well as the inclusion of higher harmonics into the d-wave gap function. These two effects nicely support the percolative nature of the superconductivity as well as the growing importance of magnetic interaction below the optimum doping level.

The opposite effect of oxygen isotope substitution and pressure on T^* can be qualitatively explained by theoretical models including phonon-mediated mechanisms of the pseudogap formation.[10–12] However, lattice fluctuation alone cannot reproduce the observed downward shift of T^* under pressure application, since pressure also modifies the spin degrees of freedom. We therefore conclude on the basis of our experimental results that a theoretical approach should contain both lattice as well as antiferromagnetic fluctuations as supported by recent calculations of oxygen isotope effects in high-T_c cuprates, which started from the t-J scenario and included at the same time the coupling of the electronic degrees of freedom to a Jahn-Teller Q_2-type mode.[70]

ACKNOWLEDGMENTS

This work was performed at the Swiss Spallation Neutron Source SINQ, Paul Scherrer Institut (PSI), Villigen, Switzerland. Stimulating discussions with K.A. Müller and M. Sigrist as well as financial support by the Swiss National Science Foundation through both the Project No. 20-66948.01 and the NCCR MaNEP project are gratefully acknowledged.

*Electronic address: petra.haefliger@physik.unizh.ch. Present address: Physik-Institut der Universität Zürich, Winterthurerstr. 190, CH-8057 Zürich, Switzerland.

[1] See, e.g., T. Timusk and B. Statt, Rep. Prog. Phys. **62**, 61 (1999).
[2] See, e.g., B. Batlogg and C. Varma, Phys. World **13**(2), 33 (2002); V. M. Lokatex, R. M. Quick, and S. G. Sharapov, Phys. Rep. **349**, 1 (2001).
[3] A. Lanzara, G. M. Zhao, N. L. Saini, A. Bianconi, K. Conder, H. Keller, and K. A. Müller, J. Phys.: Condens. Matter **11**, L541 (1999).
[4] D. Rubio Temprano, J. Mesot, S. Janssen, A. Furrer, K. Conder, H. Mutka, and K. A. Müller, Phys. Rev. Lett. **84**, 1990 (2000).
[5] D. Rubio Temprano, J. Mesot, S. Janssen, K. Conder, A. Furrer, A. Sokolov, V. Trounov, S. M. Kazakov, J. Karpinski, and K. A. Müller, Eur. Phys. J. B **19**, 5 (2001).
[6] D. Rubio Temprano, K. Conder, A. Furrer, H. Mutka, V. Trounov, and K. A. Müller, Phys. Rev. B **66**, 184506 (2002).
[7] A. Furrer, K. Conder, P. S. Häfliger, and A. Podlesnyak, Physica C **408-410**, 773 (2004).
[8] F. Raffa, T. Ohno, M. Mali, J. Roos, D. Brinkmann, K. Conder, and M. Eremin, Phys. Rev. Lett. **81**, 5912 (1998).
[9] G. V. M. Williams, J. L. Tallon, J. W. Quilty, H. J. Trodahl, and N. E. Flower, Phys. Rev. Lett. **80**, 377 (1998).
[10] S. Andergassen, S. Caprara, C. Di Castro, and M. Grilli, Phys. Rev. Lett. **87**, 056401 (2001).
[11] A. Bussmann-Holder, J. Supercond. **13**, 773 (2000).

[12] L. P. Gor'kov, J. Supercond. **13**, 765 (2000).
[13] H. Keller, Struct. Bonding (Berlin) **114**, 143 (2005).
[14] G. M. Zhao, K. Conder, H. Keller, and K. A. Müller, J. Phys.: Condens. Matter **10**, 9055 (1998).
[15] G. M. Zhao, H. Keller, and K. Conder, J. Phys.: Condens. Matter **13**, R569 (2001).
[16] J. P. Franck, J. Jung, M. A.-K. Mohamed, S. Gygax, and G. I. Sproule, Phys. Rev. B **44**, 5318 (1991).
[17] R. Khasanov, A. Shengelaya, E. Morenzoni, M. Angst, K. Conder, I. M. Savić, D. Lampakis, E. Liarokapis, A. Tatsi, and H. Keller, Phys. Rev. B **68**, 220506(R) (2003).
[18] R. Khasanov, D. G. Eshchenko, H. Luetkens, E. Morenzoni, T. Prokscha, A. Suter, N. Garifianov, M. Mali, J. Roos, K. Conder, and H. Keller, Phys. Rev. Lett. **92**, 057602 (2004).
[19] A. Shengelaya, H. Keller, K. A. Müller, B. I. Kochelaev, and K. Conder, Phys. Rev. B **63**, 144513 (2001).
[20] G.-H. Gweon, T. Sasagwa, S. Y. Zhou, J. Graf, H. Takagi, D.-H. Lee, and A. Lanzara, Nature (London) **430**, 187 (2004).
[21] E. Pytte, Phys. Rev. B **10**, 4637 (1974).
[22] M. Mali, J. Roos, D. Brinkman, H. Keller, A. V. Dooglav, Y. A. Sakhratov, and A. V. Savinkov, J. Supercond. **15**, 511 (2002).
[23] M. Mali, J. Roos, H. Keller, J. Karpinski, and K. Conder, Phys. Rev. B **65**, 184518 (2002).
[24] T. Machi, M. Kosuge, N. Koshizuka, and H. Yamada, in *Advances in Superconductivity IX*, edited by S. Nakayima and M. Murakami (Springer, Berlin, 1996), pp. 111–114.
[25] L. J. Shen, C. C. Lam, V. Anand, and S. H. Li, Physica C **341-348**, 929 (2000).
[26] E. V. L. de Mello, M. T. D. Orlando, J. L. González, E. S. Caixeiro, and E. Baggio-Saitovich, Phys. Rev. B **66**, 092504 (2002).
[27] P. S. Häfliger, A. Podlesnyak, K. Conder, and A. Furrer, Europhys. Lett. **73**, 260 (2006).
[28] P. S. Häfliger, A. Podlesnyak, K. Conder, E. Pomjakushina, and A. Furrer, Europhys. Lett. **67**, 1018 (2004).
[29] A. Podlesnyak., P. S. Häfliger, K. Conder, and A. Furrer, J. Phys.: Condens. Matter **17**, S801 (2005).
[30] G. T. Trammell, Phys. Rev. **92**, 1387 (1953).
[31] S. W. Lovesey and U. Staub, Phys. Rev. B **61**, 9130 (2000).
[32] A. T. Boothroyd, Phys. Rev. B **64**, 066501 (2001).
[33] A. T. Boothroyd, A. Mukherjee, and A. P. Murani, Phys. Rev. Lett. **77**, 1600 (1996).
[34] D. Rubio, J. Mesot, K. Conder, S. Janssen, H. Mutka, and A. Furrer, J. Supercond. **13**, 727 (2000).
[35] B. Roessli, P. Fischer, M. Guillaum, J. Mesot, U. Staub, M. Zolliker, A. Furrer, E. Kaldis, J. Karpinski, and E. Jilek, J. Phys.: Condens. Matter **6**, 4147 (1994).
[36] J. Mesot and A. Furrer, J. Supercond. **10**, 623 (1997).
[37] J. Mesot and A. Furrer, *Neutron Scattering in Layered Copper-Oxide Superconductors*, edited by A. Furrer (Kluwer, Dordrecht, 1998), p. 335.
[38] See, e.g., H. Alloul, T. Ohno, and P. Mendels, Phys. Rev. Lett. **63**, 1700 (1989).
[39] R. E. Walstedt and W. W. Warren, Jr., Science **248**, 1082 (1990).
[40] J. Korringa, Physica (Utrecht) **16**, 601 (1950).
[41] N. Bulut and D. J. Scalapino, Phys. Rev. B **45**, 2371 (1992).
[42] J. Mesot, P. Allenspach, U. Staub, A. Furrer, H. Mutka, R. Osborn, and A. Taylor, Phys. Rev. B **47**, 6027 (1993).
[43] H. Ding, T. Yokoya, J. C. Campuzano, T. Takahashi, M. Randeria, M. R. Norman, T. Mochiku, and K. Kadowski, Nature (London) **382**, 51 (1996).
[44] J. Mesot, G. Böttiger, H. Mutka, and A. Furrer, Europhys. Lett. **44**, 498 (1998).
[45] M. Ido, M. Momono, and M. Oda, J. Low Temp. Phys. **117**, 329 (1999).
[46] H. J. H. Smilde, A. A. Golubov, Ariando, G. Rijnders, J. M. Dekkers, S. Harkema, D. H. A. Blank, H. Rogalla, and H. Hilgenkamp, Phys. Rev. Lett. **95**, 257001 (2005).
[47] M. R. Norman, H. Ding, M. Randeria, J. C. Campuzano, T. Yokoya, T. Takeuchi, T. Takahashi, T. Mochiku, K. Kadowski, P. Guptasarma, and D. G. Hinks, Nature (London) **392**, 157 (1998).
[48] J. Mesot, M. R. Norman, H. Ding, M. Randeria, J. C. Campuzano, A. Paramekanti, H. M. Fretwell, A. Kaminski, T. Takeuchi, T. Yokoya, T. Sato, T. Takahashi, T. Mochiku, and K. Kadowaki, Phys. Rev. Lett. **83**, 840 (1999).
[49] A. P. Schnyder, A. Bill, C. Mudry, R. Gilardi, H. M. Rønnow, and J. Mesot, Phys. Rev. B **70**, 214511 (2004).
[50] K. Conder, Mater. Sci. Eng., R. **R32**, 41 (2001).
[51] P. Fischer *et al.*, Physica B **276-278**, 146 (2000).
[52] W. E. Fischer, Physica B **234-236**, 1202 (1997).
[53] J. Mesot, S. Janssen, L. Holitzner, and R. Hempelmann, J. Neutron Res. **3**, 293 (1996).
[54] Th. Strässle, M. Divǐs, J. Rusz, S. Janssen, F. Juranyi, R. Sadykov, and A. Furrer, J. Phys.: Condens. Matter **15**, 3257 (2003).
[55] P. G. Radaelli, D. G. Hinks, A. W. Mitchell, B. A. Hunter, J. L. Wagner, B. Dabrowski, K. G. Vandervoort, H. K. Viswanathan, and J. D. Jorgensen, Phys. Rev. B **49**, 4163 (1996).
[56] P. M. Singer, A. W. Hunt, A. F. Cederström, and T. Imai, Phys. Rev. B **60**, 15345 (1999).
[57] A. Furrer, P. Bruesch, and P. Unternährer, Phys. Rev. B **38**, 4616 (1988).
[58] P. Fischer, K. Kakurai, M. Steiner, K. N. Clausen, B. Lebech, F. Hulliger, H. R. Ott, P. Brüsch, and P. Unternährer, Physica C **152**, 145 (1988).
[59] M. T. Hutchings, in *Solid State Physics*, edited by F. Seitz and D. Turnbull (Academic, New York, 1964), Vol. 16, p. 227.
[60] A. Ino, T. Mizokawa, K. Kobayashi, A. Fujimori, T. Sasagawa, T. Kimura, K. Kishio, K. Tamasaku, H. Eisaki, and S. Uchida, Phys. Rev. Lett. **81**, 2124 (1998).
[61] H. Takahashi *et al.*, Phys. Rev. B **50**, 3221 (1994).
[62] M. C. Murayama, Y. Iye, T. Enomoto, N. Môri, Y. Yamada, T. Matsumoto, Y. Kubo, Y. Shimakwa, and T. Manako, Physica C **183**, 277 (1991).
[63] N. Momono, T. Matsuzaki, M. Oda, and M. Ido, J. Phys. Soc. Jpn. **71**, 2832 (2002).
[64] J. L. Tallon and J. W. Loram, Physica C **349**, 53 (2001).
[65] P. W. Anderson, Science **235**, 1196 (1987).
[66] P. W. Anderson, P. A. Lee, M. Randeria, T. M. Rice, N. Trivedi, and F. C. Zhang, J. Phys.: Condens. Matter **16**, R755 (2004).
[67] A. Furrer, D. Rubio Temprano, J. Mesot, K. Conder, and K. A. Müller, J. Supercond. **15**, 361 (2002).
[68] P. G. Radaelli, C. U. Segre, D. G. Hinks, and J. D. Jorgensen, Phys. Rev. B **45**, 4923 (1992).
[69] L. Gor'kov and V. Kresin, J. Supercond. **13**, 239 (2000).
[70] A. Bussmann-Holder and H. Keller, e-print cond-mat/0409738 (unpublished).